

Power laws in a 2-leg ladder of interacting spinless fermions.

L. G. Caron* and C. Bourbonnais†

*Département de physique and Centre de recherche sur les propriétés électroniques de matériaux avancés (CERPEMA),
Université de Sherbrooke, Sherbrooke, QC J1K 2R1, Canada.*

(Dated: October 31, 2018)

We use the Density-Matrix Renormalization Group to study the single-particle and two-particle correlation functions of spinless fermions in the ground state of a quarter-filled ladder. This ladder consists of two chains having an in-chain extended Coulomb interaction reaching to third neighbor and coupled by inter-chain hopping. Within our short numerical coherence lengths, typically reaching ten to twenty sites, we find a strong renormalization of the interchain hopping and the existence of a dimensional crossover at smaller interactions. We also find power exponents for single-particle hopping and interchain polarization consistent with the single chain. The total charge correlation function has a larger power exponent and shows signs of a crossover from incoherent fermion hopping to coherent particle-hole pair motion between chains. There are no significant excitation energies.

PACS numbers: 71.10.Pm, 71.27.+a, 05.10.Cc

I. INTRODUCTION

The theory of quasi-one-dimensional conductors^{1,2,3,4,5,6,7,8,9} has shown that there are dimension-specific aspects not observed in conventional three-dimensional solids. Aside from the interaction dependent power law behavior of single-particle and pair response functions and the well documented spin-charge separation, there is the renormalization of the transverse hopping whose impact on the description of real materials is much debated^{10,11}. As discussed in length in Ref. 3, strong Coulomb interactions can dramatically reduce the effective value of the transverse hopping and retard the dimensionality crossover from a one-dimensional (1D) to a two- or three-dimensional conductor. The simplest theoretical testing ground for this idea is a 2-leg ladder consisting of interacting spinless fermions on two chains coupled by a transverse hopping t_{\perp} . It is in principle possible to study the putative renormalization of t_{\perp} . This has been done using various approaches, among which exact diagonalization¹², momentum-space renormalization¹³, and bosonization^{14,15,16,17}. In all these papers, renormalization of the interchain hopping is confirmed. What we propose is a numerical calculation of this two-chain problem at quarter-filling using the efficient density-matrix renormalization group^{18,19,20,21} (DMRG) in order to directly measure power law exponents and the effective value of the interchain hopping. Although the DMRG has recently been tried²² on spinless fermions, the analysis focused on a half-filled ladder and the nearest neighbor current correlations.

We shall first present the model Hamiltonian we shall be using throughout and, second, the proposed DMRG procedure. Thirdly, we shall validate our approach on the single chain situation. We thereafter present the results for two chains and discuss the results in the light of the various theoretical treatments. A brief summary follows.

II. HAMILTONIAN

We shall use the model Hamiltonian proposed by Capponi *et al.*¹² for two quarter-filled chains of spinless fermions that interact within each chain through a finite extent Coulomb potential and can hop between chains through the hopping term t_{\perp} . The Hamiltonian is

$$H = - \sum_{j,\beta} \left(c_{j+1,\beta}^{\dagger} c_{j,\beta} + h.c. \right) + \sum_{j,\beta,r} V(r) n_{j+r,\beta} n_{j,\beta} - t_{\perp} \sum_j \left(c_{j,1}^{\dagger} c_{j,2} + h.c. \right) \quad (1)$$

where $c_{j,\beta}$ annihilates a fermion at site j ($j = 1, \dots, N$) on chain β ($\beta = 1, 2$), $n_{j,\beta}$ is the occupancy at the same site, and $V(r) = 2V/(r+1)$ is the intra-chain interaction between first, second, and third neighboring sites ($r = 1, 2, 3$) with V as the interaction strength. We have set the intra-chain hopping element equal to one.

We have chosen an interaction to third nearest neighbor because the work of Capponi showed that the single-fermion exponent α , characterizing the long-range single-chain inter-site transfer function

$$C1(j, r) = \langle c_{j+r}^{\dagger} c_j \rangle \propto r^{-(1+\alpha)}, \quad (2)$$

can become very large ($\alpha \lesssim 1.5$ for $V \leq 6$). This power exponent is responsible for the perhaps better known singularity in the momentum distribution at the Fermi level of Luttinger liquids. In the limit of small α , one has $[n(k) - n(k_F)] \sim |k - k_F|^{\alpha} \text{sign}(k_F - k)$. Large values of α will be easily observed and are expected to lead to much more important effects on the effective value of t_{\perp} . Large values of α are also synonymous with strong variations in the stiffness K . The two are related through the relation

$$\alpha = \frac{1}{2} (K + 1/K - 2) \quad (3)$$

for spinless fermions on a chain. Consequently, the power law exponents of the various response functions, which are related to K , will also be strongly affected.

III. DENSITY-MATRIX RENORMALIZATION GROUP

The exact diagonalization of Eq.(1) by Capponi¹² was for short chains of up to twenty sites. Needless to say that some sort of extrapolation procedure, finite-size scaling in this case, was needed to obtain ground state information in the thermodynamic limit. We have chosen to use the DMRG since much longer chains can be studied. This, in principle at least, should take the system much closer to the thermodynamic limit and do away with the requirement of performing a finite-size scaling analysis.

Another shortcoming of short chain lengths has to do with a “dimensionality” crossover in the interchain hopping^{3,14,15}. For temperatures or frequencies larger than approximately $|t_\perp|$, the chains do not “see” the interchain hopping, which is incoherent or diffusive, and they are approximately independent. But in the opposite situation, the chains are tightly coupled and they form bands having transverse dispersion. Let us illustrate this in the situation of quarter filling for $V = 0$ and an even number of fermions. An exact solution to two coupled chains is available. The states are labelled by $k_m = \pi m/(N + 1)$ where $1 \leq m \leq N$ and have energy $E_\pm(k_m) = -2 \cos(k_m) \pm |t_\perp|$. For $t_\perp = 0$, all levels up to $m = m_F = N/4$ are filled with $N/2$ fermions. There is no interchain hopping. As $|t_\perp|$ increases, this remains so until $E_+(k_{m_F}) = E_-(k_{m_F+1})$, that is until $|t_\perp| \approx (\pi v_F/2)/(N + 1)$. Here v_F is the Fermi velocity equal to $\sqrt{2}$ in our units. At this point there is a sudden change in interchain hopping since the two top levels below the Fermi level are E_- states. The total interchain hopping energy E_\perp is now $-2|t_\perp|$. The next jump occurs at $|t_\perp| \approx 3(\pi v_F/2)/(N + 1)$ when $E_+(k_{m_F-1}) = E_-(k_{m_F+2})$, after which $E_\perp = -4|t_\perp|$. At a given $|t_\perp|$, the jumps occur at $N \approx [(\pi v_F/2t_\perp)(2p - 1) - 1]$ for $p = 1, 2, \dots$, when $E_\perp = -2p|t_\perp|$. Taking $|t_\perp| = 0.1$ for example, $(\pi v_F/2t_\perp) = 10\pi/\sqrt{2} \sim 22$. This is a large value. It is therefore difficult to attempt finite-size scaling or the DMRG under such conditions. One can only hope of reaching the thermodynamic limit for $N \gg (\pi v_F/2t_\perp)$. This behavior is surely attenuated in the presence of the Coulomb interaction which scrambles the spectrum. But short chains remain unpredictable because of the discrete energy spectrum. Thus the longer chain lengths obtainable with the DMRG would circumvent this potential numerical distortion. In the event that t_\perp renormalizes to much smaller values than the bare one, this crossover phenomenon might even prove cumbersome to the DMRG. In order to avoid potential problem we chose to use the finite system algorithm proposed by White^{19,20,21}, projecting out the ground state of the superblock. At a given V , we started with the procedure with largest value of $|t_\perp|$ we wished to consider, 0.5 in all cases, and then gradually decreased its value using the previous solution as a seed. For each set of parameters, the iterations stopped when the discontinuity in the ground state energy and the excitation energy E_x

at mid-course, when all block information has just been refreshed, were judged acceptable. This was typically for 3 iterations. We used open boundary conditions since periodic boundary conditions lead to unacceptably large truncation errors.

Let us lastly comment on the number of central sites to use in the DMRG algorithm. The long-range character of the Coulomb interaction complicates the calculations. For two inner double-sites (two sites on each chain), the computation resources (execution time and memory requirements) scale roughly as $4^2(N_B)^4$ where N_B is the number of sites in each of the side blocks. This comes from the coupling of the two blocks through $V(r = 3)$. If one instead chooses to have three inner double-sites, the blocks no longer couple and the resources scale as $4^3 48(N_B)^3$ which comes from the coupling of the inner sites to each block. We have found that the resources are similar for $N_B \sim 100$ in qualitative agreement with this crude analysis. We have used two inner sites for the values of $N_B = 42, 64, 96$ and three for $N_B = 128$.

IV. SINGLE CHAINS

It is of utmost importance to test our DMRG procedure on simpler single-chain problems. There are two delicate aspects that need to be validated, both linked to the open-ended boundary conditions. The first one has to do with the value of N that can be chosen for a specific band filling. The second one concerns the numerical treatment that must be done on the data in order to generate information for infinite-length chains.

A. Chain length and band filling

The sensitivity to open ended boundary conditions can be illustrated for a chain of spinless fermions with an interaction extending only to nearest neighbor sites ($V(r) = V\delta_{r,1}$) near half filling. The ground state and the excitation energy are completely different for the $N = 2N_f$ and $N = 2N_f - 1$ situations, where N_f is the number of fermions. Fig. 1 shows the ground state excitation energy in both situations for a calculation with $N_B = 42$ block states and $N = 151, 152$. Although N_B seems small, the truncation error was nevertheless smaller than 3×10^{-7} for an open ended chain. A gap develops for the case $N = 151$ and $N_f = 76$ but not for the other. As for the ground states, they show a site occupancy $n_j = \bar{n} + A_m \cos(\pi j - \theta_j)$ that is alternating between a large and a small value. This basic pattern is to be expected for a broken symmetry state with a repulsive interaction. But while the modulation phase θ_j is a constant for $N = 151$, it varies for $N = 152$. We find $\theta \sim \pi j/N$ in a calculation where the interaction is introduced right away in the first iteration of the finite size algorithm (sudden turn on) but $\theta \sim 3\pi j/N$ when a first set of iterations is done with $V = 0$ and then V is

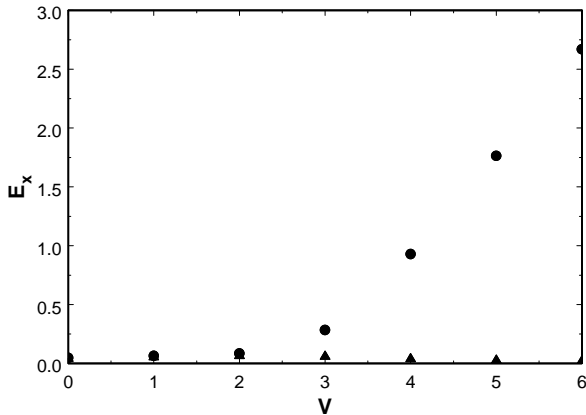


FIG. 1: Ground state excitation energy of a half-filled chain of spinless fermions with nearest-neighbor interaction strength V . The number of sites is 151 (circles) and 152 (triangles).

introduced in the second set of iterations, using the first one as seed (gradual turn on). The ground state energy is lowest in the latter situation. The alternating occupancy in the ground state can be understood by looking at the large V limit when one might expect the fermions to segregate on alternating sites [...1010...]. It is the boundary conditions that will determine the modulation phase. For $N = 151$, one would expect $|101\dots101\rangle$ to be the stablest situation, with $\theta_j = 0$, and this would explain a uniform modulation and the excitation gap. But for $N = 152$, the chain will spontaneously create a kink soliton (phase shift of π from end to end) $|101\dots010\rangle \Rightarrow |101\dots001\rangle$ which can then redistribute itself and lead to a gapless excitation situation. This is found for the sudden turn on. However, it is also possible for the chain to generate additional kink-antikink excitations. The results for the gradual turn on confirm this and show that this situation is more stable. Just how many kink-antikink pairs would be generated is impossible to figure out with the DMRG. Curiously, the DMRG seems unable to yield an unambiguous ground state when $N = 2N_f$ for open boundary conditions.

The single-chain Hamiltonian we have just been studying is akin to the XXZ problem for a spin 1/2 chain²³. This spin Hamiltonian can be transformed, using the Wigner-Jordan transformation, into our problem with $J_z = V$ and $J_x = J_y = 2$ except for end terms $\frac{1}{2}V(n_1 + n_N)$, involving the first and last sites, that occur for open boundary conditions. The XXZ chain is known to develop a gap for $J_z > J_x$, that is for $V > 2$. For $N = 2N_f$, the ground state is degenerate, $|101\dots010\rangle$ and $|010\dots101\rangle$, has no soliton because of the end site repulsion and has a gap. It is the pressure applied to the fermions by the end terms that insures the presence of an excitation energy and a uniform modulation amplitude in this situation. In the case of our ladder with $N = 2N_f - 1$, it is the shorter length that adds extra pressure to the fermions and similarly leads to a gapped

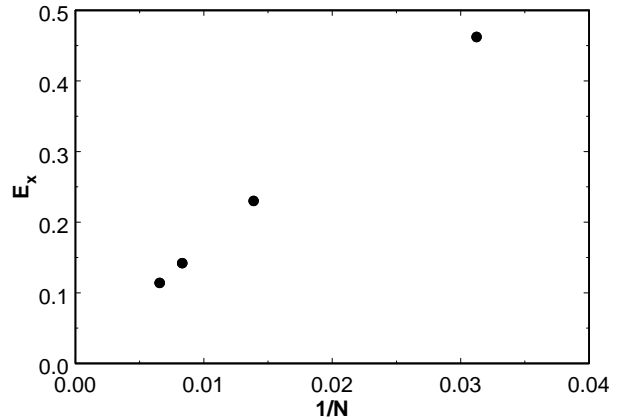


FIG. 2: Ground state excitation energy of a quarter-filled chain of spinless fermions with third-neighbor interaction strength $V = 6$ as a function of the reciprocal of the chain length.

situation.

In view of this dichotomy with respect to occupation near half filling, it is legitimate to ask if this sensitivity persists near quarter filling. To this end, we did a limited incursion with *gradual turn on* at $V = 6$, $N_f = 38$, $N = 149, 150, 152$, and for first neighbor ($r = 1$), second neighbor ($r = 1, 2$), and third neighbor ($r = 1, 2, 3$) interactions. The ground state energy per fermion for a given interaction range decreases slightly with N . The effective constraining “pressure” when $N = 4N_f - m$ ($m = 1, 2, 3$) can explain this. The ground state excitation energy E_x remains small going from 0.046 to 0.11 as the range increases and is insensitive to N . Judging from Fig. 1, this is not a significant gap and is due to the finite length of the chains. Fig. 2 shows the excitation energy as a function of the inverse of the chain length for a third-neighbor interaction strength $V = 6$ and $N_B = 42$. The extrapolated gap for $N \rightarrow \infty$ is indeed negligibly small. There is, however, a variation of the modulation of the site occupancy of the form $n_j = \bar{n} + A_m \cos(\pi j/2 - \theta_j)$. Indeed, for $N = 152$, we find $\theta_j = (3\pi j)/(2N)$. This situation is the generalization of the one seen above for half filling and gradual turn on condition, the quantum of phase shift being $\pi/2$ instead of π . What this θ_j means is that the Fermi momentum is downward shifted from its exact quarter-filled value $k_F = (\pi/4)(1 - 3/N)$ due to fermions being pushed to the ends. The question spontaneously arises as to any possible detrimental effect of such modulation on the correlation functions. We shall answer this in the following subsection.

B. Data processing

We have just found that a modulation in the site occupancy results from the open boundary conditions which pin fermions at the end site and lead to a broken sym-

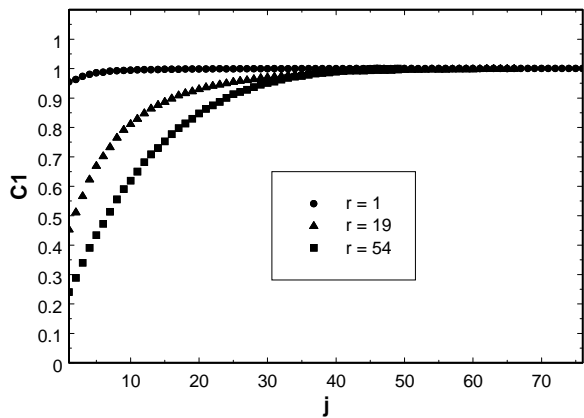


FIG. 3: Doubly averaged single-fermion transfer function for a quarter-filled chain normalized to its value at the maximum as a function of the site of origin j . The plots stop at $j = (N - r)/2$. We have chosen $N = 152$, $N_B = 42$, $V = 6$, and three different transfer distances (see legend).

metry state. This modulation obviously makes it non trivial to get occupancies (the \bar{n}) or correlation functions resembling those for periodic boundary conditions or an infinite chain. Taking the occupancy as an example, for the quarter-filled situation, it can be seen that the modulated part $A_m \cos(\pi j/2 - \theta_j)$ can be made less annoying by averaging over the natural four site cycle. Indeed, if we define for instance $\bar{n}_j = \frac{1}{4} \sum_{i=0}^3 n_{j+i} = \bar{n} - A_m [\cos(\pi j/2 - \theta_j) + \sin(\pi j/2 - \theta_j)] (3\pi/4N)$, one immediately sees that the modulation is reduced by a factor of order N^{-1} . A second averaging, $\bar{\bar{n}}_j = (1/16) \sum_{i=0}^3 \sum_{m=0}^3 n_{j+i+m}$, would further reduce it by another N^{-1} . One can thus, for all practical purposes, remove the effect of the modulation for long chains, thus our choice of long chain lengths. We have used throughout what follows double averaging with interactions reaching to third neighbor at quarter filling.

But, unfortunately, the open boundary conditions produce yet another deformation. The smoothed quantities, like \bar{n} , are not global quantities but rather local ones. They vary along the chain, the more so the closer a site is to the ends. We can illustrate this by looking at the profile of the single-fermion transfer function $\overline{C1}(j, r)$ defined in Eq. (2) using double averaging, $N = 152$, $V = 6$ and $N_B = 42$. The plots are for $1 \leq j \leq (N - r)/2$ since the results are symmetrical about this last value. Fig. 3 shows this function for $r = 1, 19, 54$, normalized to $\overline{C1}((N - r)/2, r)$. The healing distance increases with r and is at the scale of r . It is quite obvious that the ends can have dramatic effects at the larger values of r . We have used this optimal positioning at $j = (N - r)/2$ in all calculations reported below of quantities dependent on r .

But are averaging and optimal positioning sufficient to obtain results corresponding to the thermodynamic limit? We can check this by extracting the power law

exponent of the inter-site transfer function $C1(r) = \overline{C1}((N - r)/2, r)$. In order to do so, one needs to have an analytic function with which to fit the data for $C1(r)$. From the known form of the single-particle Green's function of a Luttinger liquid^{5,9}, this function would read as

$$C1(r) = \left(\frac{\bar{n} \sin(k_F r)}{k_F r} \right) \left(\frac{1}{1 + (r/\Lambda)^2} \right)^{\alpha/2} \quad (4)$$

where k_F is the Fermi momentum. This form was obtained from bosonization and Λ is a characteristic cutoff parameter. This form, however, has to be modified to account for the DMRG procedure on a finite lattice. We find that the gap associated with a finite N introduces a numerical coherence length ξ in much the same way that a temperature $T \propto N^{-1}$ would. We thus propose the substitution^{6,24} $r \rightarrow \xi \sinh(r/\xi)$ and thus the following form

$$C1(r) = \left(\frac{\bar{n} \sin(k_F r)}{k_F \xi \sinh(r/\xi)} \right) \left(\frac{1}{1 + (\xi \sinh(r/\xi)/\Lambda)^2} \right)^{\alpha/2} \quad (5)$$

We calculated $C1(r)$ for a chain having $N = 152$, $V = 1, 2, \dots, 6$, and $N_B = 42$. The truncation error was less than 10^{-8} . The fitted parameters, in the range $1 \leq r \leq 100$, are in Table I. It is seen that $k_F \sim (\pi/4)(1 - 3/N)$ as expected. The power law exponents α are those found by Capponi *et al.*¹² although they seem systematically larger by 5-8 %. The coherence lengths are satisfactorily quite large, giving added credibility to our fitting function. The Pearson correlation coefficient²⁶ between ξ and E_x^{-1} is 0.986 indicating that the two parameters are strongly correlated. Finally, the cutoff Λ is of order one, the lattice parameter, as one would expect for fermions on a lattice. It can thus be concluded that the fitting function, Eq. (5), is quite satisfactory, with an error margin of order 5 %, considering the large number of adjustable parameters. The thermodynamic limit is thus recovered albeit slightly handicapped by a numerical coherence length ξ . Now how does the $2k_F$ charge density fluctuation response function turn out? We also calculated the correlation function $C2(r) = C2((N - r)/2, r)$ where

$$C2(j, r) = \langle (n_{j+r} - \langle n_{j+r} \rangle) (n_j - \langle n_j \rangle) \rangle \quad (6)$$

This function measures the correlation between occupancy (proportional to charge) fluctuations on site j and $(j + r)$. It has the advantage of getting at the true fluctuation correlations in a broken symmetry state. There are, however, many wavenumber contributions to two-fermion Green's functions^{5,9}. One expects $q = 0$ and $4k_F$ contributions aside from the sought $2k_F$ correlations. We observe that $C2(r)$ has a fast oscillating part $B_f(r)$ and a slow modulation amplitude $A_s(r)$, such that $C2(r) \approx A_s(r)B_f(r)$. What we did was to exponentiate the data $C2(r) \exp(-\ln(|A_s(r)|))$, do a fast Fourier transform, remove the unwanted contributions, and unexponentiate back the remaining $2k_F$ contribution. For

TABLE I: Various parameters calculated for a quarter-filled chain at different values of V and for $N_B = 42$.

V	E_x	k_F	α	K	ξ	Λ	K_c	d_c
1	0.049	0.78	0.106	0.63	81	1.5	0.67	100
2	0.064	0.78	0.27	0.49	76	1.2	0.52	87
3	0.076	0.78	0.49	0.39	65	1.2	0.42	69
4	0.088	0.78	0.76	0.31	59	1.3	0.35	59
5	0.101	0.77	1.08	0.25	53	1.4	0.29	53
6	0.114	0.77	1.50	0.21	47	1.5	0.20	43

spinless fermions, the charge correlation function at $2k_F$ behaves like r^{-2K} where K is the stiffness defined in Eq. (3). The $2k_F$ filtered data could best be fit by the analytical form

$$C2(r) = C \cos(2k_F r + \varphi_c) r^{-2K_c} \exp(-r/d_c), \quad (7)$$

which has a coherence length d_c that is related to the excitation gap in a finite chain. The resulting power law exponent and coherence length are also shown in Table I. K_c is within 5 % of the calculated values of K obtained by inverting Eq. (3). d_c seems closely correlated to ξ and both to E_x^{-1} . The Pearson correlation coefficient between d_c and ξ is 0.995 and 0.984 between d_c and E_x^{-1} . The two coherence lengths ξ and d_c enter the fitting functions of Eqs. (5) and (7) in quite different ways. This probably stems from the different role the block states $|\psi^B\rangle$ play in matrix element storage, off diagonal with respect to total block occupation \mathfrak{N}^B in single-fermion functions $\langle \psi^B(\mathfrak{N}_1^B) | c_j | \psi^B(\mathfrak{N}_2^B) \rangle$ but diagonal for the charge correlations $\langle \psi^B(\mathfrak{N}_1^B) | n_j | \psi^B(\mathfrak{N}_1^B) \rangle$. One last comment concerns the $q = 0$ charge correlations. We found no evidence for this contribution in our data possibly because of the specific quantity we chose to calculate in Eq. 6.

We wish to point out an interesting observation we made on the raw (unaveraged) occupation n_j near the ends. We can fit the occupation by the relation

$$n_j \approx \bar{n} + n_0 \cos(2k_F j + \phi) (j)^{-K_c} \quad (8)$$

where $\bar{n} = 0.25$ and $0.25 \lesssim n_0 \lesssim 0.4$. A similar observation has recently been reported in Ref. 25. The broken symmetry state resulting from the pinning at the chain ends forces the local occupancy variation $\langle \delta n_j \rangle$, where $\delta n_j = n_j - \bar{n}$, to be equal to the root mean square fluctuation $\sqrt{\langle \delta n_0 \delta n_j \rangle}$.

We wish to end this subsection by examining the situation for $N_B = 10$. Why such a small number of block states? We have already stated that our calculations were made with $N_B \leq 128$. This is at the limit of our computational capabilities. If the chains were independent, this would be equivalent to having some 10 block states per chain, which is not large indeed. At such small values of N_B , we had to introduce another coherence length ξ_c for the charge correlations,

$$C2(r) = C \cos(2k_F r + \varphi_c) \times (\xi_c \sinh(r/\xi_c))^{-2K_c} \exp(-r/d_c). \quad (9)$$

TABLE II: Various parameters calculated for a quarter-filled chain at different values of V and for $N_B = 10$.

V	E_x	α	ξ	K_c	ξ_c	d_c
1	0.20	0.10	19	0.65	30	22
2	0.23	0.26	15	0.50	31	19
3	0.24	0.48	16	0.41	35	22
4	0.26	0.75	17	0.33	34	21
5	0.27	1.10	17	0.26	32	21
6	0.29	1.50	15	0.21	32	21

We used a fitting procedure which weighed more heavily the data for $r \lesssim \xi$ so as to be able to recover key parameters with values close to those at $N_B = 42$. Truncation errors run typically at the level of a few times 10^{-5} . This is considerably larger than for $N_B = 42$. Table II gives some of the parameters of the fit. We have used the values of Λ of Table I. α and K_c compare favorably. The ground state excitation energy has appreciably increased and the coherence length has shortened. They are rather featureless, a signature of the small number of block states. Note that $\xi_c \sim d_c$ is somewhat ‘‘elastic’’ in the sense that its value can drift significantly without marked effect (within the 5 % error bar) on the fit.

V. COUPLED CHAINS

Now that we have acquired sufficient experience and confidence in data management, we can tackle the study of two coupled chains. One final observation is warranted. We found that convergence of our DMRG algorithm could only be achieved relatively quickly for an odd number of fermions $N_f = (2N_{f0} + 1)$. This can be understood in view of our discussion in Section IV A. First of all, fermions are pushed to the ends by the Coulomb repulsion. The fermion occupancies on both chains thus start site-synchronized at the ends. Secondly, the transverse hopping favors out of phase occupancies on the chains. Fig. 4 illustrates this. It shows the on-site charge ($\langle n_{j,1} \rangle + \langle n_{j,2} \rangle$) and polarization ($\langle n_{j,1} \rangle - \langle n_{j,2} \rangle$) that is typical of the broken-symmetry ground state. The larger V is, the more pronounced the out of phase character (polarization) is and the larger the $4k_F$ charge component. This behavior can be achieved more easily in a state in which one chain has one extra fermion. The chain with $(N_{f0} + 1)$ fermions is more compressed and cannot easily sustain solitons. But then, the chain with N_{f0} fermions can easily accommodate a kink-antikink pair which then allows the inner part of this chain to be out of phase with the ends and with the other chain. Broken symmetry states also have the advantage of focusing the computational resources to a single non-degenerate state instead of splitting them between degenerate states thus decreasing the numerical coherence length. We have thus chosen to do our calculations for $N = 150$. Our truncation error varies from 5×10^{-5} for $N_B = 42$ to 5×10^{-6} for the

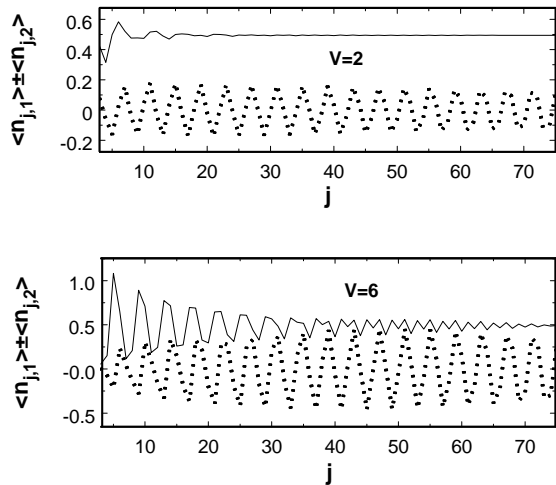


FIG. 4: On-site charge (full line, + sign) and polarization (dotted line, - sign) in typical broken symmetry states at $V = 2, 6$ and for $t_{\perp} = 0.5$.

larger values $N_B = 128$. We have kept the Λ values of the single chain.

We shall first look at single-fermion behavior and then at some two-fermion correlation functions.

A. Single-fermion transfer function

The perturbative renormalization group formulation in Ref. 3 presented a unified description of the renormalization of t_{\perp} and the generation of interchain couplings in quasi-1D solids. Although the basic elements are present, the treatment is perturbative and subject to caution for large interactions. The bosonization approaches have the potential to do better in this respect since the single-chain interacting spinless fermion problem has an exact solution.

Let us then examine the predictions of bosonization. There are two key treatments which look at our Hamiltonian from two different perspectives. Nersesyan *et al.*¹⁵ (NLK) bosonize the chain fermion operators $c_{j,\beta}$, whereas Yoshioka and Suzumura¹⁴ (YS) do so with the band operators

$$c_{j,\sigma} = (c_{j,1} + \sigma c_{j,2}) / \sqrt{2}. \quad (10)$$

Here $\sigma = \pm 1$ is the band index. One has $k_{\perp} = (1 - \sigma)(\pi/2)$. The procedure yields two separated sectors, polarization and occupation, that, by analogy to a chain of spins $\frac{1}{2}$ in a magnetic field $\propto t_{\perp}$, are labelled spin and charge.

In NLK, there is spin-charge separation and the Coulomb interaction is absorbed within the stiffnesses K_c and K_s . Here K_c has the same value as for a single chain. t_{\perp} appears in the spin sector and acts as the generator of interchain two-fermion couplings G and \tilde{G}

corresponding to particle-hole and particle-particle pair hopping. The renormalization group (RG) equations for G reads $G' = 2(1 - K_s)G + (K_s - \tilde{K}_s)\tau^2$, where $\tau = |t_{\perp}| \Lambda / (2\pi u_s)$, u_s is the spin excitation velocity, $\tilde{K}_s = 1/K_s$, and the prime indicates the derivative with respect to $\ell = \ln(\max(\omega/E_0, T/E_0, v_F k/E_0))$ where E_0 is the starting energy scale. This is discussed in Refs. 1 and 3. The equation for \tilde{G} is obtained by the substitution $\tilde{K}_s \leftrightarrow K_s$. Note that $G(\ell = 0) = \tilde{G}(0) = 0$. This RG equation is different from Yakovenko's¹⁶ whose τ^2 term is larger by a factor $8\pi^2$. This does not change the qualitative behavior of the equations, only the numbers. Furthermore, it is more in line with the coefficients of the RG equations in Ref. 3. The RG also renormalizes t_{\perp} , $\tau' = (2 - \Delta_s)\tau$ where $\Delta_s = \frac{1}{2}(K_s + \tilde{K}_s)$, and K_s is governed by $(\ln K_s)' = \frac{1}{2}(\tilde{K}_s^2 \tilde{G}^2 - K_s G^2)$. Note that one has $K_s(\ell = 0) = K_c$. There are additional contributions of order τ^2 to this last equation³, a fact acknowledged by NLK, but which will remain unexplored by us. When G reaches strong coupling ($G \sim 1$) then a gap opens in the spin sector and only the charge sector contributes to power laws.

In YS, there is also spin-charge separation for small t_{\perp} . But the authors point out that this is no longer true for large transverse hopping, when the Fermi velocities for the two bands are appreciably different. This should be kept in mind as our values of $t_{\perp} \geq 0.1$ should qualify. The charge sector behaves essentially as in NLK, with $\eta \equiv K_c$. The spin sector, however, transforms the Coulomb interaction into two inter-band couplings $g_{2\phi+}$ and $g_{2\phi-}$ such that the spin stiffness $\eta_{\phi} = 1$ at $\ell = 0$. This dichotomy between spin and charge sectors is satisfactory for small V . The RG equations (when corrected for typographical errors) yield solutions qualitatively similar to NLK for $t_{\perp}(\ell)$. But it rapidly becomes annoying at large interactions since the spin sector quickly, too quickly, goes to strong coupling when $g_{2\phi+}$ or $g_{2\phi-} \sim 1$ and develops a gap. It then appears that the NLK approach should do better before the single-fermion dimensionality crossover and YS after the crossover, when bands have formed.

Let us now focus on the predictions of these models for the transverse hopping as a function of length scale $x(\ell) = \exp(\ell)$. We first start with NLK at $\ell = 0$. The RG equations will switch to YS once the dimensionality crossover is reached, when $\tau(\ell_x) \sim (2\pi)^{-1}$, via the mapping proposed in NLK. We have chosen this value as it produces crossovers at scales comparable with the ones of Bourbonnais³ and YS. With this choice, the renormalized transverse hopping

$$t_{\perp}(\ell) = (2\pi u_s / \Lambda) \tau(\ell) \exp(-\ell) \approx 2\pi v_F \tau(\ell) / x(\ell)$$

leads to a dimensionality crossover at

$$\begin{aligned} t_{\perp}(\ell_x) &= (2\pi u_s / \Lambda) \tau(\ell_x) \exp(-\ell_x) \\ &\approx v_F \exp(-\ell_x) = v_F / x(\ell_x), \end{aligned} \quad (11)$$

in which we have set $\Lambda = 1$ and $u_s = v_F$. This is the result of Bourbonnais for the crossover. Fig. 5(a) shows the

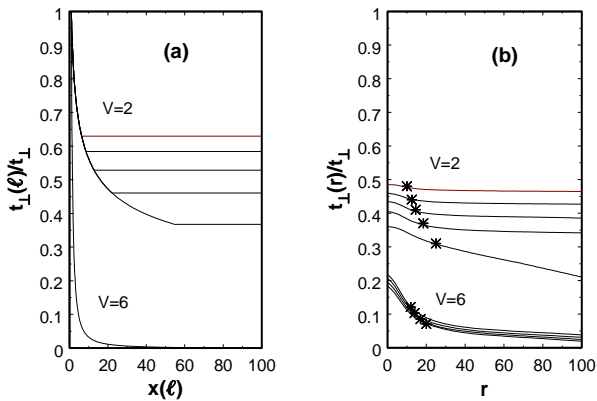


FIG. 5: Transverse hopping as a function of the length scale normalized to the bare value for various situations. The curves for $V = 2$ are for $0.5 \geq t_{\perp} \geq 0.1$ from top to bottom. (a) NLK bosonization results. The $V = 6$ curves are for all values of t_{\perp} . (b) DMRG results. The $V = 6$ curves are for $0.5 \geq t_{\perp} \geq 0.2$, from top to bottom, respectively. The stars are set at the values of the coherence length ξ .

results for the renormalized transverse hopping $t_{\perp}(\ell)$ at both intermediate ($V = 2$) and strong ($V = 6$) Coulomb interactions. This was obtained using the $K_s = K$ values in Table I at $\ell = 0$. On the one hand, the $V = 2$ results are typical of small V and large t_{\perp} and clearly show the dimensionality crossover. The “ladder” diagram is typical of this crossover regime. The renormalized hopping after the crossover satisfies the relation

$$(t_{\perp}(\ell_x)/t_{\perp}) \propto (t_{\perp})^{\alpha/(1-\alpha)} \quad (12)$$

as proposed by Bourbonnais and verified by Capponi. On the other hand, the $V = 6$ curves for different t_{\perp} all superimpose, a signature of the confined regime ($\alpha > 1$).

The DMRG calculations we now present were taken at $N_B = 96$. The following band transfer functions were calculated

$$C1(r, \sigma) = \overline{C1((N-r)/2, r, \sigma)} \quad (13)$$

where $C1(j, r, \sigma) = \langle c_{j+r, \sigma}^{\dagger} c_{j, \sigma} \rangle$. Each of these two $C1(r, \sigma)$ was fitted with Eq. (5). The fit could only be made by allowing the $k_F(r, \sigma)$ which characterize the bands σ to vary as a function of r , a situation not seen in single chains. This is how the renormalization of the transverse hopping manifests itself most directly. We could then calculate the renormalized transverse hopping from

$$t_{\perp}(r) \approx [k_F(r, \sigma = 1) - k_F(r, \sigma = -1)]/v_F. \quad (14)$$

The results for this last quantity are reproduced in Fig. 5(b). The four upper curves for $V = 2$ clearly show the “ladder” characteristic of the crossover situation. This crossover, from Eq. (11), is approximately at $r_x \approx v_F/t_{\perp}(r_x)$ which has been reached before the coherence

length is reached for $t_{\perp} \geq 0.2$. The renormalized transverse hopping is also rather flat for $r > r_x$. This is not the case for the $t_{\perp} = 0.1$ curve which has a “drooping” (negative slope) characteristic. This intermediate value of V has this nice property of showing both the crossover and its absence due to numerical coherence. Moreover, the predicted renormalization law of Eq. (12) gives a value $\alpha \sim 0.26$ for the top four curves, a value in excellent agreement with the single chain one. This is somewhat accidental as the same analysis performed on the $V = 1$ data for $0.2 \leq t_{\perp} \leq 0.5$ yields a value of $\alpha \sim 0.14$, somewhat larger than its value in a single chain. The problem, if there is one, may lie with Eq. (14) which does not account for the change in Fermi velocity that occurs when the values of $k_{\perp} = 0, \pi$ are appreciably different (large t_{\perp}) or due to renormalization. One must bear in mind that the DMRG is on a lattice and the fermion energy is far from the linear dispersion of the RG. Non-universal band edge effects (pre-RG) might be considerable and this might explain the discrepancy at the sizeable values of t_{\perp} we have used. We find no clear evidence for a crossover at $V \geq 3$ as $\xi < r_x$ and the $t_{\perp}(r)$ curves do not flatten out at r_x .

The $V = 6$ curves are bunched together and show confinement. This is in qualitative agreement with bosonization. Our results indicate that the coherence length sets the scale for the evolution of the transfer function. Further evolution, such as crossovers, are blocked at distances beyond ξ . The splitting, albeit small, of the different $V = 6$ curves is caused by just this effect. The coherence lengths are shorter for the larger values of t_{\perp} thus leading to larger, that is less renormalized, values of $t_{\perp}(\ell)$.

It is important to understand the connection between $t_{\perp}(r)$ and $t_{\perp}(\ell)$. $t_{\perp}(r)$ can be viewed, from Ref. 3, as an average over all momentum scales $k \lesssim k_r \equiv 2\pi/r$. It is thus an average of $t_{\perp}(\ell)$ over $\ell \lesssim \ln(v_F k_r/E_0)$. Thus clearly $t_{\perp}(r = 0) = \overline{t_{\perp}(\ell)} \neq t_{\perp}(\ell = 0)$. That is why $t_{\perp}(r = 0)$ is larger than $t_{\perp}(r)$ yet smaller than the bare value t_{\perp} .

Fig. 6(a) shows the fitted values for α for both $k_{\perp} = 0, \pi$. They are surprisingly nearly independent of t_{\perp} or of the existence or not of a dimensionality crossover. This is not expected from bosonization which would predict a variation of $K_s(\ell)$ and thus of α . This is perhaps a consequence of the absence of true spin-charge separation. YS also predict a change in exponent at the crossover. Fig. 6(b) shows the average numerical coherence lengths for $k_{\perp} = 0, \pi$. The coherence lengths monotonically decrease at constant V as t_{\perp} increases. Curiously, ξ is smallest at $V = 2, 3$. We will come back to this in the next subsection.

Quite obviously, it would be futile to study the scaling behavior of these quantities with the chain length since ξ is much shorter. But it would be possible to study the scaling with $(N_B)^{-1}$ which acts like a temperature. In an attempt to better understand our results, we thus repeated the calculations at other values of N_B . Fig. 7

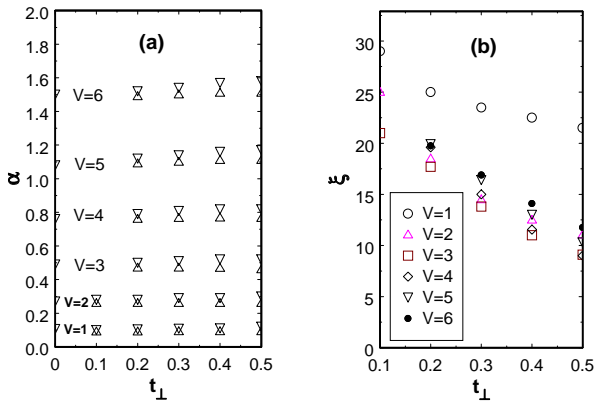


FIG. 6: Fitted values for the DMRG transfer function at different transverse hopping and Coulomb interaction strengths. (a) Power law exponent results. The downward pointing triangles are for $k_{\perp} = \pi$ while the upward pointing ones are for $k_{\perp} = 0$. (b) Mean values of the numerical coherence length.

shows the scaling behavior of the ground state excitation energy and the reciprocal of the coherence length for $V = 2$. The gap is seen to extrapolate, as $N_B \rightarrow \infty$, to small values of E_x compatible with $N = 150$. There is thus no indication of an energy gap. But ξ^{-1} no longer correlates well with E_x in contrast to results for single chains. As a matter of fact, the extrapolated value increases quasi-linearly with t_{\perp} . The same behavior is found for all values $V \geq 1$. Fig. 8 shows the $N_B \rightarrow \infty$ extrapolated inverse coherence lengths for $V = 2$ and $V = 6$ as well as the reciprocal of the threshold values to strong coupling coming from numerical solutions of the bosonization equations. We see there is a tight correlation between bosonization and DMRG behaviors with t_{\perp} , though the length scales are different, in both situations with or without a crossover. This suggests the coherence lengths are affected by the oncoming strong coupling regime at which our fitting formula, Eq. (5), would no longer be valid.

B. Two-particle correlations

Following Eq. 6, we define the on-site charge ($\nu = +$) and polarization ($\nu = -$) correlation functions $C2(r, \nu) = C2((N - r)/2, r, \nu)$, where

$$C2(j, r, \nu) = \langle (n_{\nu, j+r} - \langle n_{\nu, j+r} \rangle) (n_{\nu, j} - \langle n_{\nu, j} \rangle) \rangle, \quad (15)$$

and

$$n_{\pm, j} = n_{j, 1} \pm n_{j, 2}. \quad (16)$$

What should we expect for the power law exponents

$$C2(r, \nu) \propto r^{-K_{\nu}} \quad (17)$$

characterizing these correlation functions? It is quite clear that as $t_{\perp} \rightarrow 0$, the chains become independent and

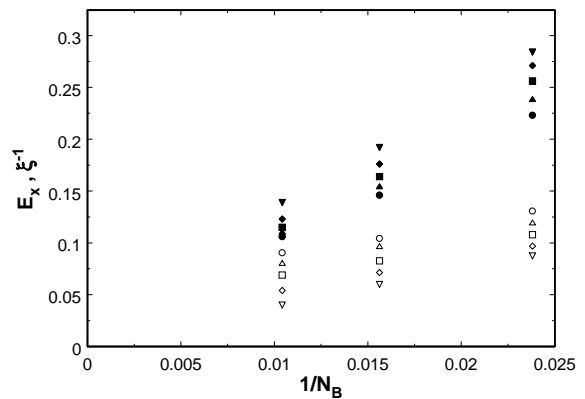


FIG. 7: Ground state excitation energy E_x (full symbols) and inverse coherence length ξ^{-1} (empty symbols) as a function of N_B^{-1} for $V = 2$. The curves are for $0.5 \geq t_{\perp} \geq 0.1$ from bottom to top, for E_x , and top to bottom for ξ^{-1} .

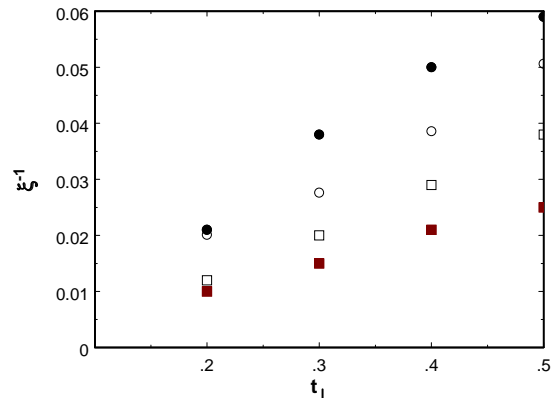


FIG. 8: Inverse coherence length extrapolated to an infinite number of block states, circles, and reciprocal of the thresholds to strong coupling calculated from the bosonization equations, squares, as a function of the transverse hopping. The results for $V = 2$, full symbols, and $V = 6$, empty symbols, are shown.

one should have $K_{\nu} = K_c + K_s = 2K_c$. This is consistent with NLK. From the band perspective, the approach of YK predicts $K_+ = (\eta + \eta_{\phi})$ and $K_- = (\eta + 1/\eta_{\phi})$ when there is no gap. Since $\eta_{\phi} > 1$ for repulsive interactions, one should expect $K_+ > K_-$.

We have calculated these correlation functions and tried fitting them to forms reminiscent of Eq. (9). The polarization correlation function behaves nicely and can be fitted with

$$C2(r, -) = C_- \cos((k_F(r, 1) + k_F(r, -1))r + \varphi_-) \times (\xi_- \sinh(r/\xi_-))^{-K_-} \exp(-r/d_-) \quad (18)$$

using the filtering procedure explained in the data processing of single-chain correlations. The exponents K_- are essentially those of the charge correlations of single chains as witnessed in Fig. 9. Again, this is unexpected. It is as if $(\eta + 1/\eta_{\phi})$ or $(K_c + K_s)$ remained nearly constant. This behavior is like the one observed for the sin-

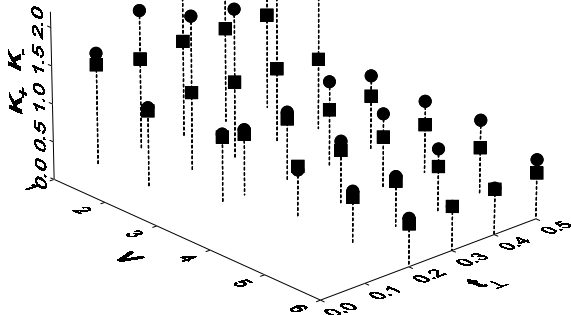


FIG. 9: Power law exponents for charge, full circles, and polarization, full boxes, for various values of V and t_{\perp} .

gle particle exponent α . This points to the breakdown of spin-charge separation for a highly non-linear dispersion. As for ξ_{-} and d_{-} , we find they are generally larger than ξ , sometimes by a sizeable factor, and also fairly “elastic” as observed for single chains.

The charge correlation function proved a bit more subtle to fit. The charge correlations generally decrease much faster than the polarization correlations. They rapidly become quite noisy when they reach the limits set by the truncation error. This can easily be monitored on a logarithmic plot of the amplitude of $C2(r, +)$ as a function of r . There is a sudden break in the general linearlike decrease. The range of values in which a function having an amplitude of the type proposed in Eq. (18) can be appropriate is often limited to $r \lesssim 30$ when the coherence lengths are small. We have extended our calculations to $N_B = 128$ for a few cases as a check of the sturdiness of our calculations. It is mostly ξ_{-} that is affected by a noticeable increase. Curve fitting with many parameters can thus become delicate and leads to large uncertainties which we estimate at 10% for K_{+} . We found that we could fit $C2(r, +)$ with a form equivalent to Eq. (18) with $\nu = +$ instead of $\nu = -$ for all cases $V \geq 3$. The fast Fourier transform reveals only one broad “ $2k_F$ ” wavenumber. K_{+} is always of the same size or a bit larger than K_{-} in this chain-like regime as can be seen in Fig. 9. For those situations $V \leq 2$, the fast Fourier analysis reveals two wavenumbers associated with $2k_F(r, 1)$ and $2k_F(r, -1)$. We sometimes fitted the most prominent wavenumber or sometimes both, when the separation was not big enough, with a form that combines contributions of both bands (see Eq. 10)

$$C2(r, +) = \sum_{\sigma} C_{+, \sigma} \cos(2k_F(r, \sigma)r + \varphi_{+, \sigma}) \times (\xi_{+} \sinh(r/\xi_{+}))^{-K_{+}} \exp(-r/d_{+}) .(19)$$

As can be seen from Fig. 9, K_{+} is appreciably larger than K_{-} in the low V regime. We found ξ_{+} and d_{+} to be somewhat smaller than ξ and still “elastic”. It is

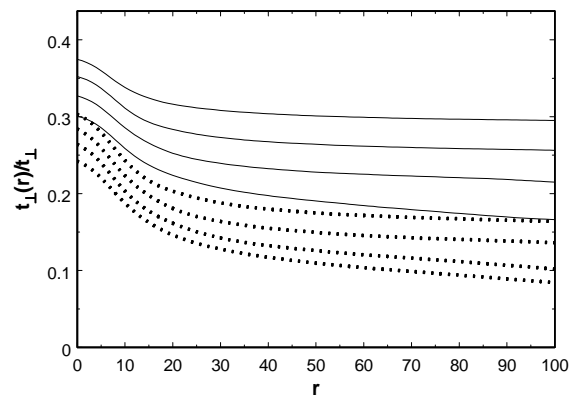


FIG. 10: Transverse hopping as a function of the length scale normalized to the bare value for $V = 3$ (full lines) and $V = 4$ (dotted lines). The curves are for $0.5 \geq t_{\perp} \geq 0.2$ from top to bottom.

quite apparent from Fig. 9 that there is a discontinuity in K_{+} going from $V = 2$ to $V = 3$, with values dropping from 2 to 1. This behavior is, we believe, intrinsic to the coupled chains and is not a result of short coherence lengths since these are of the same size for $V = 2, 3$. It indicates a crossover from a single-fermion dominated behavior, when the charge fluctuations are propagated through independent band-like particle and hole motion showing two wavenumbers in the charge response function, to a pair behavior, when the fluctuations are carried by particle-hole pairs having chain-like character sharing a common wavenumber. Such a crossover was deduced by Capponi¹² in the same range of values of V . In this crossover region, there is fierce competition between single-fermion behavior and coherent pair motion. The computer resources are shared between the two competing behaviors and this explains the shorter coherence lengths in the crossover region. In spite of the domination of the pair motion, the transverse hopping is not necessarily confined as Fig. 10 shows. There are no clear crossovers at the larger t_{\perp} , using the criteria discussed in the previous subsection, but the hopping is considerable and decreases only slowly with distance. There may well be coexistence between coherent interchain pairing and some sort of interband single particle behavior before the strong-coupling limit is reached, a possibility raised by NLK.

It should finally be mentioned that, as was described in Section IV B for single chains, we find a broken symmetry state in which the total on-site occupancy variation $\langle \delta n_{+, j} \rangle$ is proportional to the square root of the charge correlation amplitude $(\xi_{+} \sinh(j/\xi_{+}))^{-K_{+}/2} \exp(-j/2d_{+})$ near the ends.

VI. SUMMARY

Let us now sum up the more important findings on the quarter-filled double-chain problem. Our working hypothesis is that the fitting functions and the data treatment we have used for the analysis of one- and two-particle functions, which were validated for single chains, can safely be carried over to two coupled chains.

1. The central result, which motivated this whole study, is the confirmation of strong renormalization of the inter-chain hopping in the presence of the Coulomb interaction V . This was measured by monitoring the difference in the Fermi momentum of the two bands beyond the dimensionality crossover. The extent of the renormalization is much stronger than expected from the RG or bosonization at small V . It is considerable at the larger V . It is most likely going to zero as can be concluded by observing the trend in $t_{\perp}(r)/t_{\perp}$ which decreases with t_{\perp} . The proposed crossover law, Eq. (12), was seen to be only approximately valid when the crossover exists. It is probably our definition, Eq. (14), and band edge effects that are responsible.

2. The single-fermion transfer function power-law ex-

ponent α and the polarization correlation function exponent K_{-} were seen to be essentially those of the single chain. This is interpreted as a sign of possible violation of spin-charge separation.

3. The charge correlation function shows superposition of two wavenumbers and has an exponent K_{+} that is twice as large as the one for polarization for $V \leq 2$. This indicates the existence of a crossover from independent particle-hole motion to correlated pair motion between $V = 2$ and $V = 3$.

4. The ground state excitation energy, when extrapolated to $N_B \rightarrow \infty$, is as expected for a finite system of 150 sites. The coupled chains thus remain gapless. There are also indications, in the same limit, of possible strong coupling regimes as inferred from the linear-like t_{\perp} dependence of the extrapolated inverse coherence lengths, much in the same way that bosonization predicts.

The rather short numerical coherence lengths we have encountered with the DMRG, although expected from the study on single-chains, did put some stress on the curve fitting procedures. This resulted in fairly large errors in our exponents.

* Electronic address: caron@physique.usherb.ca

† Electronic address: cbourbon@physique.usherb.ca

¹ J. Solyom, *Adv. Phys.* **28**, 201 (1979).

² Y. A. Firsov, Y. N. Prigodin, and C. Seidel, *Phys. Rep.* **126**, 245 (1985).

³ C. Bourbonnais and L. G. Caron, *Int. J. Mod. Phys. B* **5**, 1033 (1991).

⁴ C. Bourbonnais, in *Les Houches, Session LVI (1991), Strongly interacting fermions and high- T_c superconductivity*, edited by B. Doucot and J. Zinn-Justin (Elsevier Science, Amsterdam, 1995), p. 307.

⁵ J. Voit, *Rep. Prog. Phys.* **58**, 977 (1995).

⁶ V. J. Emery, in *Highly Conducting One-Dimensional Solids*, edited by J. T. Devreese, R. E. Evrard, and V. E. van Doren (Plenum Press, New York, 1979), p. 247.

⁷ S. Brazovskii and Y. Yakovenko, *Sov. Phys. JETP* **62**, 1340 (1985).

⁸ H. J. Schulz, in *Proceedings of Les Houches Summer School LXI*, edited by E. Akkermans, G. Montambaux, J. Pichard, and J. Zinn-Justin (Elsevier, Amsterdam, 1995), p. 533.

⁹ H. J. Schulz, G. Cuniberti, and P. Pieri, in *Field Theories for Low-dimensional Condensed Matter Systems*, edited by G. Morandi, P. Sodano, A. Tagliacozzo, and V. Tognetti (Springer, 2000).

¹⁰ C. Bourbonnais and D. Jérôme, in *Advances in Synthetic Metals, Twenty Years of Progress in Science and Technology*, edited by P. Bernier, S. Lefrant, and G. Bidan (Elsevier, New York, 1999), pp. 206–261, arXiv:cond-mat/9903101.

¹¹ S. Biermann, A. Georges, A. Lichtenstein, and T. Giamarchi, cond-mat/0107633.

¹² S. Capponi, D. Poilblanc, and E. Arrigoni, *Phys. Rev. B* **57**, 6360 (1998).

¹³ M. Fabrizio, *Phys. Rev. B* **48**, 15838 (1993).

¹⁴ H. Yoshioka and Y. Suzumura, *J. Phys. Soc. Japan* **64**, 3811 (1995).

¹⁵ A. A. Nersisyan, A. Luther, and F. V. Kusmartsev, *Phys. Lett. A* **176**, 363 (1993).

¹⁶ V. M. Yakovenko, *JETP Lett.* **56**, 510 (1992).

¹⁷ P. Donohue, M. Tsuchiizu, T. Giamarchi, and Y. Suzumura, *Phys. Rev. B* **63**, 45121 (2001).

¹⁸ S. R. White and R. M. Noack, *Phys. Rev. Lett.* **68**, 3487 (1992).

¹⁹ S. R. White, *Phys. Rev. Lett.* **69**, 2863 (1992).

²⁰ S. R. White, *Phys. Rev. B* **48**, 10345 (1993).

²¹ I. Peschel, X. Wang, M. Kaulke, and K. Hallberg, eds., *Density-Matrix Renormalization: a New Numerical Method in Physics*, vol. 528 of *Lecture Notes in Physics* (Springer, Heidelberg, 1999).

²² K. Yonemitsu, *Synth. Met.* **120**, 845 (2001).

²³ F. D. M. Haldane, *Phys. Rev. Lett.* **45**, 1358 (1980).

²⁴ H. Frahm and V. E. Korepin, *Phys. Rev. B* **42**, 10553 (1990).

²⁵ S. R. White, I. Affleck, and D. J. Scalapino, cond-mat/0111320.

²⁶ The Pearson correlation coefficient is equal to the covariance of the two variables divided by the products of their standard deviations.